Microchemical Journal 225 (2026) 118092

Contents lists available at ScienceDirect

Microchemical Journal

journal homepage: www.elsevier.com/locate/microc

Development of a peptide-based KIM-1 biosensor utilizing computationally designed CCT3-derived peptides

Muhammad Syafiq Mohd Razib [a], Shoko Tanaka [a], Noor Syamila [a,b], Muhamad Arif Mohamad Jamali [c], Amir Syahir Amir Hamzah [d], Shinya Ikeno [a,*]

[a] Department of Biological Functions Engineering, Graduate School of Life Science and System Engineering, Kyushu Institute of Technology, Kitakyushu Science and Research Park, Kitakyushu, Fukuoka, Japan
[b] Biogenes Technologies Sdn Bhd, Jalan Maklumat, Universiti Putra Malaysia, 43400 Serdang, Selangor, Malaysia
[c] Faculty of Science and Technology, Universiti Sains Islam Malaysia, Bandar Baru Nilai, Nilai, Negeri Sembilan, Malaysia
[d] Department of Biochemistry, Faculty of Biotechnology and Biomolecular Sciences, Universiti Putra Malaysia, Serdang, Selangor, Malaysia

ARTICLE INFO

Keywords:
Kidney injury molecule-1
T-complex protein 1 subunit gamma
MBP-CCT3-BP04
Peptide biosensor
In silico

ABSTRACT

The kidney injury molecule-1 (KIM-1) serves as a well-recognized biomarker for kidney injury, making the establishment of accurate and sensitive detection methods highly valuable for clinical applications. This research involved computational design and analysis of protein-binding peptide fusion; MBP-CCT3-BP03 and MBP-CCT3-BP04 were engineered to bind to KIM-1. Because peptides are generally small in size, both designed binding peptides were fused with maltose binding protein (MBP) to assist in their expression and biosensor fabrication. The affinity study and the development of biosensors were conducted electrochemically. The molecular docking binding affinity of CCT-BP03 and CCT3-BP04 against KIM-1 was predicted at −8.8 kJ/mol and − 8.1 kJ/mol respectively, while their calculated MM/PBSA were recorded at −45.70 kJ/mol and − 36.1 kJ/mol, respectively. In addition. The MD simulation structural analysis reveals that MBP-CCT3-BP04 exhibits better structural stability and folding during the 100 ns simulation while interacting with KIM-1, hence it was chosen for the development of the KIM-1 biosensor. Under optimal conditions, the developed biosensor showed a linear correlation of MBP-CCT3-BP04 related to the concentration of KIM-1 with a detection limit of 1.02 ng/mL, where it falls within the clinical range of KIM-1 in urine. The designed MBP-CCT3-BP04 also demonstrates high specificity and selectivity in both the spiked buffer and the simulated urine sample. Overall, this research establishes the viability of using computational procedure in designing binding peptides as well as employing protein-binding peptide fusion approach for biosensor development. This approach provides a practical framework for creating cost-effective and reliable KIM-1 detection platforms that could have significant clinical utility.

1. Introduction

Modern lifestyles have contributed to the global rise of non-communicable diseases, including acute kidney injury (AKI), which can progress into chronic kidney disease (CKD). Its increasing prevalence is largely driven by aging populations, low income, urban lifestyles, and dietary habits [1] associated with chronic conditions such as hypertension and diabetes [2,3]. Recent research examining 2021 data shows that chronic kidney disease linked to elevated body mass index resulted in approximately 418,400 fatalities and 10.42 million Disability-Adjusted Life Years (DALYs) globally. The condition affects men at higher rates than women. Since 1990, CKD-related mortality has increased by 354%, with the most rapid rise occurring in regions with low sociodemographic development [4]. The disease impacts over 674 million individuals worldwide, with elevated blood glucose levels (accounting for 36% of DALYs) and high BMI (representing 23.4% of DALYs) identified as the primary risk factors [5]. These findings highlight the critical importance of developing accessible point-of-care testing and diagnostic tools for early detection and monitoring of chronic kidney disease risk.

CKD is characterized by a persistent reduction in glomerular filtration rate and/or elevated levels of albuminuria, indicating long-term kidney damage [6]. It is often asymptomatic in its early stages and frequently goes undetected until significant kidney damage has

* Corresponding author.
E-mail address: ikeno@life.kyutech.ac.jp (S. Ikeno).

https://doi.org/10.1016/j.microc.2026.118092
Received 9 January 2026; Received in revised form 23 February 2026; Accepted 9 April 2026
Available online 18 April 2026

occurred. Late-stage diagnosis is typically associated with irreversible loss of kidney function, posing a substantial burden on healthcare systems, particularly in underdeveloped and developing countries [7]. Moreover, strategies for early detection and prevention remain underutilized in many healthcare settings [8].

Serum creatinine is commonly used as a diagnostic marker for CKD; however, its major limitation lies in its insensitivity to early kidney damage, as elevated levels typically appear only after significant loss of renal function [9]. In recent years, numerous alternative biomarkers have been investigated for their potential in the early detection of CKD. These include kidney injury molecule-1 (KIM-1), liver-type fatty acid-binding protein (L-FABP), neutrophil gelatinase-associated lipocalin (NGAL), insulin-like growth factor-binding protein 7 (IGFBP7), interleukin-18 (IL-18), tissue inhibitor of metalloproteinases-2 (TIMP-2), and proenkephalin (PENK) [10]. Additionally, non-invasive sample sources such as urine and saliva are being explored for biomarker detection to improve patient compliance and screening accessibility [11,12].

KIM-1 is a type I transmembrane glycoprotein primarily expressed in the proximal tubule of the kidney [13]. While it is minimally present in healthy kidneys, KIM-1 is rapidly upregulated in response to AKI [14]. This upregulation serves to mediate phagocytosis of apoptotic cells and cellular debris and to modulate the inflammatory response, thereby supporting tubular repair [15]. However, persistent KIM-1 expression is associated with chronic inflammation and fibrosis, contributing to the progression of CKD. KIM-1 undergoes proteolytic shedding by metalloproteinases at its mucin domain, releasing its extracellular portion into urine and serum [16]. Elevated levels of soluble KIM-1 in urine are widely recognized as a sensitive and specific early biomarker for both AKI and CKD [17].

Electrochemical biosensors have gained widespread recognition in recent years as an effective detection method due to their precision, sensitivity and versatility. Various bioreceptors such as antibodies, aptamers, enzymes, proteins, and peptides can be immobilized onto the surface of an electrode with the intention to bind to a specific target analyte [18]. The interaction between bioreceptors and their target analyte will generate signals that can be amplified and measured using electrochemical techniques [19]. In addition to that, the highly selective nature of bioreceptors towards its target analyte enables researchers to develop biosensors that are tailored for particular analytical applications. Peptide-based biosensors for instance offer several advantages over other types of bioreceptors, including high target specificity, rapid signal generation, and compatibility with miniaturized formats [20,21]. Engineered peptides can maintain binding functionality under various environmental conditions, making them well-suited for the development of biosensor.

In this study, we aimed to derive binding peptides from KIM-1 binding proteins reported in a recent proteomic analysis by Yang et al. (2023), which mapped the KIM-1 interactome using co-immunoprecipitation and mass spectrometry. The design of binding peptides against KIM-1 was primarily done using computational approach as the prediction model provides a good insight into the interaction between the two molecules at the atomic level. Apart from that, their dynamic behavior and predictive binding can be conveniently studied without the need for laborious trial-and-error methodologies. Herein, by coupling *in silico* data along with experimental procedures, the analysis provides a rational foundation for exploring T-complex protein 1 subunit gamma (CCT3)-derived peptides as potential KIM-1 ligands [22].

2. Methodology

2.1. Chemicals, reagents, and apparatus

The peptide sequence with the highest binding affinity towards KIM-1 was chosen and chemically synthesized by GenScript (Fukuoka, Japan). Sodium chloride (NaCl), potassium chloride (KCl), disodium hydrogen phosphate dodecahydrate ($Na_2HPO_4.12H_2O$), monopotassium phosphate (KH_2PO_4), N-hydroxysuccinimide (NHS), potassium ferricyanide (III) ($K_3[Fe(CN)_6]$) and potassium ferrocyanide ($K_4[Fe(CN)_6]$) were purchased from FUJIFILM Wako Pure Chemical Corporation (Osaka, Japan), Yeast extract, tryptone and N-(3-dimethylaminopropyl)-N′-ethylcarbodiimide (EDC) were acquired from Thermo Fisher Scientific (Massachusetts, USA), Pyromellitic dianhydride (PMDA) and KIM-1 protein were obtained from Sigma-Aldrich (Missouri, USA) and Elabscience Biotechnology Inc. (Texas, USA) respectively. Under optimal conditions, the binding affinity test was conducted using screen-printed carbon electrodes (SPCEs) with 4 mm diameter of working electrode purchased from DropSens (Oviedo, Spain). Meanwhile, the development of KIM-1 biosensor was fabricated on a carbon counter and working electrode (4 mm) SPCEs purchased from Biogenes Sdn. Bhd. (Serdang, Malaysia) along with a silver reference electrode, Ag/AgCl purchased from ALS (Tokyo, Japan) were utilized for the development of KIM-1 biosensor, entirely. Electrochemical analysis in this study was conducted using μStat-i 400 s Potentiostat/Galvanostat/Impedance Analyzer from Metrohm (Herisau, Switzerland).

2.2. In silico screening for peptide design template model

An existing dataset from Yang et al. [22] that identified 20 binding partner proteins through co-immunoprecipitation studies in an acute kidney injury model was utilized to identify potential KIM-1 binding proteins. All 20 proteins underwent *in silico* screening to select an appropriate template for the peptide design. The workflow for the *in silico* methodologies is summarized and presented in Fig. S1. Firstly, protein-protein molecular docking analysis was conducted using AutoDock Vina 2 software [23] to assess how KIM-1 would bind against the surface-exposed regions of each binding partner protein. The three-dimensional structures of KIM-1 (PDB ID: 5DZO) as well as the other binding partner proteins were obtained from the Protein Data Bank database. Prior to docking analysis, the protein structures were prepped using AutoDockTools software, with grid parameters and rotational freedom settings customized according to each protein's dimensions. Apart from that, molecular dynamics (MD) simulation was also performed on all binding partner protein-KIM-1 pairs to study the behavior of the protein-KIM-1 complex over time, using GROMACS software employing CHARMM36m all-atom force field to simulate native protein behavior [24–26]. Each model was solvated in the TIP3P water model with 0.15 M KCl as neutralizing ions during energy minimization. Energy minimization was first conducted using the steepest descent algorithm until the maximum force reached <1000 kJ/mol/nm. Subsequently, equilibration was performed in two phases: a 100 ps NVT ensemble using the V-rescale thermostat at 300 K, followed by a 100 ps NPT ensemble using the Parrinello–Rahman barostat at 1 bar to stabilize system density. After initial energy minimization and equilibration step, the simulations ran for 100 ns were performed with periodic boundary conditions, Particle Mesh Ewald (PME) electrostatics, and LINCS constraints applied to all covalent bonds involving hydrogen atoms to observe dynamic interactions between the proteins. The resulting molecular docking results were analyzed by the predicted binding affinity whereas the resulting MD simulation data was analyzed using Molecular Mechanics Poisson-Boltzmann Surface Area (MM/PBSA) calculations to quantify total binding energy. By coupling the initial docking binding affinity with the MM/PBSA total binding energy results, the binding protein that demonstrates the most favorable binding interactions against KIM-1 was chosen to be used as the template model for our peptide design.

2.3. Binding peptide design and in silico validation

The template protein was selected following *in silico* screening of KIM-1 and its binding partner protein among the high-performing

docking models. Next, the specific amino acid residues involved in the protein-protein interaction were identified and mapped using the PDBsum server (https://www.ebi.ac.uk/thornton-srv/databases/pdbsum/Generate.html). Herein, the residues from the binding partner protein that binds onto KIM-1 were pinpointed and highlighted in its gene map. Subsequently, a total of 5 binding peptides, namely CCT3-BP01, CCT3-BP02, CCT3-BP03, CCT3-BP04 and CCT3-BP05, with lengths ranging between 30 and 44 amino acids, were designed according to the interaction mapping. The design of each binding peptide incorporates parts of the residues identified from PDBsum analysis to ensure that the binding functionality is preserved. The three-dimensional structures of these designed binding peptides were predicted using the AlphaFold3 server (https://alphafoldserver.com/), which generated PDB files for each designed binding peptide. The reliability of the predicted 3D model was validated using PROCHECK (https://www.ebi.ac.uk/thornton-srv/software/PROCHECK) and MolProbity (https://molprobity.biochem.duke.edu/index.php). The validated structures of the designed binding peptides were then subjected to *in silico* reassessment by molecular docking and MD simulations to assess their binding behavior with KIM-1. Binding peptides that demonstrated favorable binding scores with regard to docking binding affinity and MM/PBSA total binding energy were selected for synthesis and experimental testing.

2.4. Construction of vector harboring MBP-fused peptides and its expression in E. coli expression system

pMAL-p5x vector was chosen to harbor the synthesized gene, and the recombinant plasmid was transformed into *E. coli* BL21 (DE3). The gene was ligated downstream of the malE gene thus resulting in the formation of MBP-peptide fusion protein. The construction of both plasmids is illustrated in Supplementary Fig. S2. Expression of *E. coli* BL21 (DE3) harboring pMal-p5x/CCT3-peptide was conducted under these optimizations; 1 mL of starting culture was introduced to 50 mL Luria-Bertani (LB) broth supplemented with 0.1 mM ampicillin prior to incubation at 37 °C and 160 rpm until the OD_{600} reached 0.5. Subsequently, 0.1 mM of IPTG was added and the induction was done for 6 h at a slower shaking of 120 rpm under the same temperature. The harvested culture pellet was resuspended in binding buffer (20 mM Tris-HCl, 0.2 M NaCl, 1 mM EDTA, pH 7.4) and sonicated to obtain the soluble fusion protein. The fusion protein was further purified using amylose resin (New England Biolabs, Beverly, MA, USA) packed in a gravity column. The column is equilibrated with 5 times binding buffer prior to addition of sample and the bound fusion protein were eluted with the same buffer supplemented with 10 mM maltose. Eluted fractions were pooled and dialyzed with 10 mM phosphate buffer saline (PBS) buffer, pH 7.4.

2.5. Evaluation of binding affinity of MBP-fused peptides

The binding affinity of the designed binding peptide towards KIM-1 was evaluated, where 500 pg/mL of KIM-1 was immobilized onto the working electrode of multiwalled carbon nanotubes (MWCNT) modified SPEs by EDC-NHS crosslinking, followed by blocking steps with 10 mM pyromellitic dianhydride (PMDA) and 1% bovine serum albumin (BSA) to eliminate unspecific binding. The fabricated electrode was then subjected to various concentrations of MBP-fused binding peptides, from 1 μM to 1000 μM, and the binding affinity of each MBP-fused peptides were measured by differential pulse voltammetry (DPV) analysis with potential range of −0.3 to 0.6 V with a step potential of 0.005 V, pulse amplitude of 0.2 V, and scan rate of 0.025 V/s. The signal response was plotted against the MBP-fused peptides concentration. Afterwards, the Langmuir adsorption isotherm was employed as an empirical saturation model to describe the concentration-dependent electrochemical response and to estimate the apparent surface affinity constant (K_{app}) between the MBP-fused peptide and KIM-1. It is acknowledged that the classical Langmuir model assumes homogeneous and independent binding sites, conditions that are not strictly fulfilled in the present heterogeneous multilayer electrode system. Factors such as surface heterogeneity, electrode blocking steps, mass transport effects, peptide orientation, and steric constraints may influence the observed signal response [27]. Therefore, the extracted constant is reported as K_{app} and should be interpreted as a descriptive parameter under the specific experimental conditions rather than an intrinsic thermodynamic association constant (K_a). The K_{app} values were calculated according to the following equations.

$$\frac{1}{\Delta I} = \left(\frac{1}{\Delta I_{max} K_{app}}\right) \frac{1}{[MBP - CCT3\ peptide]} + \frac{1}{\Delta I_{max}} \quad (1)$$

In this equation, ΔI refers to the experimental signal change measure by DPV analysis, [MBP-CCT3 peptide] refers to the concentration of MBP-fused peptide and ΔI_{max} refers to maximum model signal change. This equation forms a linear plot in which $\frac{1}{\Delta I_{max} K_{app}}$ is the slope and $\frac{1}{\Delta I_{max}}$ is the y-intercept. The calculated value of K_{app} and ΔI_{max} are to be integrated into the next equation.

$$\Delta I_{model} = \frac{\Delta I_{max} K_{app} [MBP - CCT3\ peptide]}{1 + K_{app} [MBP - CCT3\ peptide]} \quad (2)$$

In accordance with eq. 2, a non-linear model of the binding of MBP-fused peptide against KIM-1 was generated followed by measuring of the difference of sum square between the model and the experimental data. Integration of both non-linear fits in accordance with the Langmuir adsorption isotherm will generate a new K_{app} value which represents the binding affinity of MBP-fused peptide against KIM-1.

2.6. Fabrication of peptide-based biosensor targeting KIM-1

Development of KIM-1 biosensor was conducted on SPEs (Biogenes, Malaysia), where 10 μl of MWCNT-chitosan (MWCNT-CS) nanocomposite was coated onto the working electrode and dried overnight. Next, 10 μl of 1% starch solution was also drop-casted onto the working electrode and was left to dry overnight. The starch coating was optimized by comparing two fabrication strategies; 1) direct incorporation into the MWCNT-CS solution, and 2) sequential layer-by-layer deposition of MWCNT-CS followed by starch, where different starch concentrations were tested. The fabrication of MWCNT-CS and starch layer on the electrode serves as signal enhancer and MBP binding matrix, respectively. Thereafter, 10 μl of 15 μM MBP-CCT3-BP04 was deposited onto the working electrode and incubated for 30 min at room temperature. The layer of starch provides a functional surface to bind MBP allowing the fusion peptide part to be exposed to the upper side of the fabricated electrode. The electrode was further rinsed with distilled water to remove any unbound protein. The surface of the electrode was then undergoes dual blocking steps with 10 mM PMDA followed by 1% BSA to minimize non-specific binding and reduce the noise signals. The blocking step was carried out for 30 min each at room temperature. Post-fabrication step of the electrode involved washing of the electrode with distilled water and air-drying before storing it at 4 °C prior to electrochemical analysis. Electrochemical analysis was performed using square wave voltammetry (SWV) to evaluate the interaction between KIM-1 and the modified electrode. The measurements were carried out in 10 mM of potassium ferricyanide [$K_3Fe(CN)_6$] and potassium ferrocyanide [$K_4Fe(CN)_6 \cdot 3H_2O$] in phosphate buffer saline (pH 7.4) as the redox mediator over a potential range of −0.3 to 0.6 V with a step potential of 0.005 V, amplitude potential of 0.02 V and 10 Hz frequency.

2.7. KIM-1 detection

The analytical performance of the MBP-CCT3-BP04-based KIM-1 biosensor was assessed using square wave voltammetry (SWV) under previously optimized conditions. KIM-1 solutions at varying concentrations; from 1 pg/mL to 10 ng/mL, were applied to the working

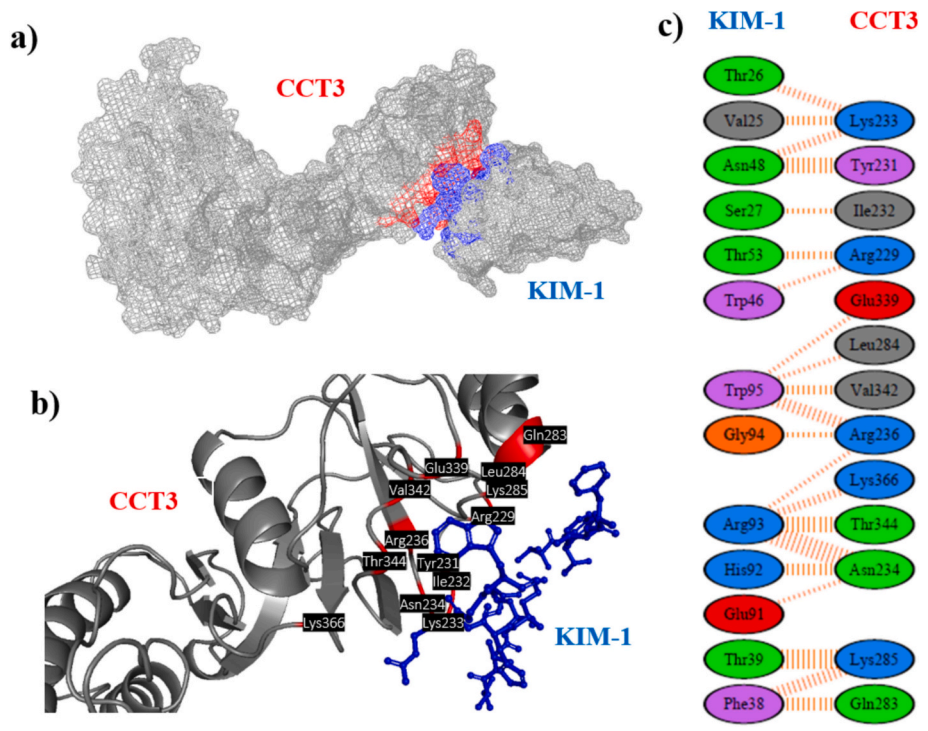

Fig. 1. Comparative representation of the KIM-1 and CCT3 binding interface. (a) PyMOL full complex view of KIM-1 docked with CCT3. (b) PyMOL structural view highlighting the spatial arrangement of these residues around the bound ligand (the residues were highlighted in red). (c) PDBsum schematic interaction map identifying key residues involved in the contacts. Together, these panels provide both schematic and structural perspectives on the binding region. (For interpretation of the references to colour in this figure legend, the reader is referred to the web version of this article.)

electrode and allowed to react for 30 min at ambient temperature, providing sufficient reaction time for MBP-CCT3-BP04/KIM-1 binding kinetics [28]. The concentrations of KIM-1 ranging from 1 pg/mL to 10 ng/mL were prepared in 10 mM PBS (pH 5.0), in accordance with optimization steps prior to electrochemical analysis. A volume of 10 μL from each concentration was pipetted onto the fabricated working electrode and incubated at room temperature for 30 min. After incubation, the unbound KIM-1 was removed by rinsing the electrode with distilled water, followed by air-drying before square wave voltammetry (SWV) analysis. Additionally, a KIM-1-spiked artificial urine sample (final concentration: 100 pM) was prepared under the same conditions to simulate real sample detection. Herein, the artificial urine was made according to the protocol described by Sarigul et al. [29]. For the selectivity study, 100 pM solutions of KIM-1 and potentially interfering proteins, C-reactive protein (CRP), Leucine-rich alpha-2-glycoprotein (LRG1), Epithelial cell adhesion molecule (EpCAM), and Secretory phospholipase A2 (sPLA2) were prepared in 10 mM PBS (pH 5.0). 10 μL of 100 pM of each protein solutions were applied to separate electrodes and subjected to the same incubation and washing protocol as described above. Batch variation, reproducibility and stability analysis of the developed sensor was expressed as relative current change (ΔI) calculated using the equations below;

Table 1
In silico binding evaluation of designed peptides with KIM-1, showing docking affinities from AutoDock Vina and MM/PBSA binding energies calculated with GROMACS (kJ/mol).

Binding peptide	Receptor	Docking Binding Affinity (kJ/mol)	MM/PBSA Total Binding Energy (kJ/mol)
CCT3-BP01	KIM-1	−4.2	−20.14
CCT3-BP02	KIM-1	−3.7	−28.38
CCT3-BP03	KIM-1	−8.8	−45.70
CCT3-BP04	KIM-1	−8.1	−36.01
CCT3-BP05	KIM-1	−3.5	−24.78

$$\text{Batch variation}: Relative\Delta I = \frac{|I_{mean\ batch\ 2} - I_{mean\ batch1}|}{I_{mean\ batch1}} \times 100 \quad (3)$$

$$\text{Reproducibility}: Relative\Delta I = \frac{Absolute\ current}{Mean\ current} \times 100 \quad (4)$$

$$\text{Stability}: Relative\Delta i = \frac{|I_{mean\ Day\ n} - I_{mean\ Day\ 0}|}{I_{mean\ Day\ 0}} \times 100 \quad (5)$$

3. Results and discussions

3.1. Computational screening identifies CCT3 as a template for peptide design

Among the proteins evaluated, CCT3 exhibited the strongest *in silico* interaction with KIM-1 based on molecular docking and MD simulations (Table S1). CCT3 displayed a predicted docking binding affinity of −12.4 kJ/mol and an MM/PBSA binding energy of −49.48 kJ/mol. In the docking model, KIM-1 was observed to interact extensively with residues within the apical domain of CCT3 (Fig. 1a, b). This binding pattern suggests potential competition with endogenous substrates or possible modulation of substrate recognition [30]. Binding interface analysis identified 13 key CCT3 residues which are Arg229, Tyr231, Ile232, Lys233, Asn234, Arg236, Gln283, Leu284, Lys285, Glu339, Val342, Thr344, and Lys366, involved in the interaction with KIM-1 (Fig. 1c). These residues formed the basis for the rational design of the five binding peptide candidates.

The structural models of the designed binding peptides were predicted using the AlphaFold server prior to *in silico* reassessment through molecular docking and molecular simulation. Sequences and structural validation (PROCHECK, MolProbity) of the designed binding peptides are shown in Table S2, Table S3 and Fig. S3. Notably, two binding peptide candidates, designated as CCT3-BP03 and CCT3-BP04, consistently exhibited favorable binding affinities, with interaction energies

Table 2
In silico binding evaluation of fusion proteins against KIM-1, showing docking affinities from AutoDock Vina and MM/PBSA binding energies calculated with GROMACS (kJ/mol).

In silico analysis	Parameter	MBP-CCT3-BP03	MBP-CCT3-BP04
MM/PBSA (kJ/mol)	VDWAALS	−98.77	−103.04
	EEL	−217.76	−526.41
	EGB	266.47	600.65
	ESURF	−14.33	−14.05
	GGAS	−316.53	−629.45
	GSOLV	252.14	586.6
	TOTAL	−64.39	−42.85
Docking Binding Affinity (kJ/mol)	–	−14.6	−14.6

Abbreviation: VDWAALS (van der Waals), EEL (Electrostatic Energy), EGB (Generalized Born Energy), ESURF (Surface Energy Contribution), GGAS (Gas-Phase Energy), GSOLV (Solvation Energy)., TOTAL (total binding energy).

and stable complex formations during simulations. CCT3-BP03 recorded a predicted docking binding affinity of −8.8 kJ/mol and calculated MM/PBSA binding energy of −45.70 kJ/mol, while CCT3-BP04 recorded a predicted docking binding affinity of −8.1 kJ/mol and calculated MM/PBSA binding energy of −36.01 kJ/mol (Table 1). The MD simulation structural analysis including root mean square deviation (RMSD), number of hydrogen bonds, radius of gyration (rGyr), and solvent accessible surface area (SASA) is also presented in supplementary Fig. S4 (a-d). Both peptides exhibited stable complex formation during simulations and were therefore selected for experimental validation. Computational analyses were used here for candidate ranking rather than quantitative prediction of binding affinity.

3.2. Structural and binding assessment of MBP-fused CCT3-derived peptides

To facilitate soluble expression and surface immobilization, CCT3-BP03 and CCT3-BP04 were fused to maltose-binding protein (MBP). MBP serves as an affinity tag for recombinant protein purification and possesses intrinsic chaperone activity, enhancing proper folding, solubility, and stability of the fused peptides [31]. Additionally, MBP's strong affinity for starch allows for controlled orientation on starch-coated electrodes, ensuring that the peptide is exposed for interaction with KIM-1. *In silico* reassessment confirmed that MBP fusion did not compromise pe o evaluate whether fusion affected peptide–target interaction, *in silico* reassessment of the MBP-fused constructs was performed. Both fusion proteins exhibited comparable docking scores (−14.6 kJ/mol). MM/PBSA calculations yielded binding energies of −64.39 kJ/mol for MBP–CCT3–BP03 and − 42.85 kJ/mol for MBP–CCT3–BP04 (Table 2). Energy decomposition analysis indicated that van der Waals interactions constituted a major favorable contribution to the calculated binding energies, particularly for MBP–CCT3–BP03. However, these interaction energies were derived from solution-phase simulations and do not account for surface immobilization constraints, steric effects, peptide orientation, or accessibility limitations inherent to the electrochemical sensing configuration. Therefore, the calculated energies and their individual components are interpreted comparatively within the computational framework rather than as quantitative predictors of experimental sensor performance.

Structural analysis over 100 ns molecular dynamics simulations

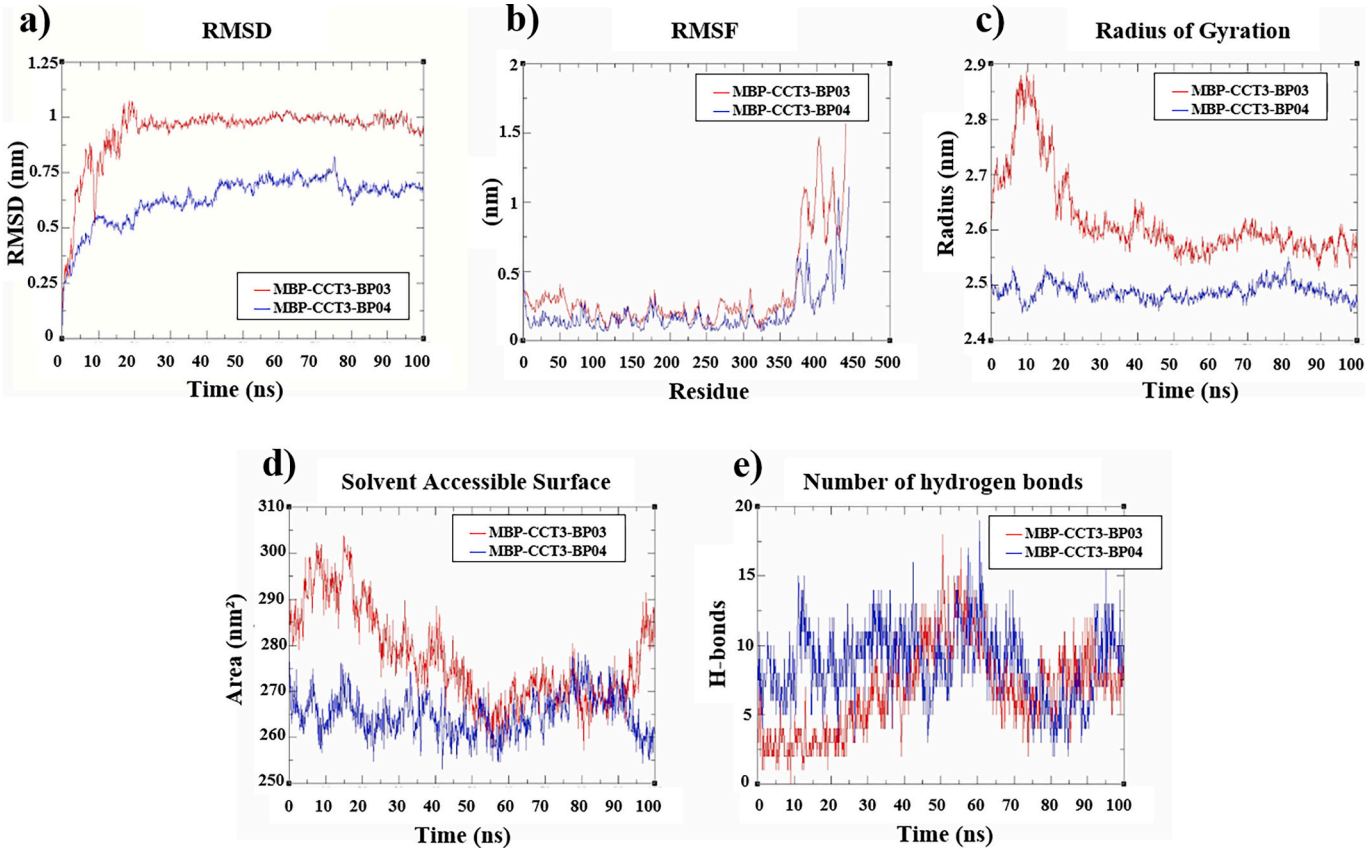

Fig. 2. Structural stability and interaction profiles of MBP–CCT3–BP03 (red) and MBP–CCT3–BP04 (blue) over 100 ns molecular dynamics simulations with KIM-1. Plots show (a) backbone RMSD, (b) RMSF per residue, (c) number of hydrogen bonds, (d) solvent accessible surface area (SASA) and (e) radius of gyration. MBP-CCT3-BP04 maintained a more compact conformation with lower RMSD, lower SASA, and higher hydrogen bonding than MBP-CCT3-BP03, indicating better stability and reduced solvent exposure. (For interpretation of the references to colour in this figure legend, the reader is referred to the web version of this article.)

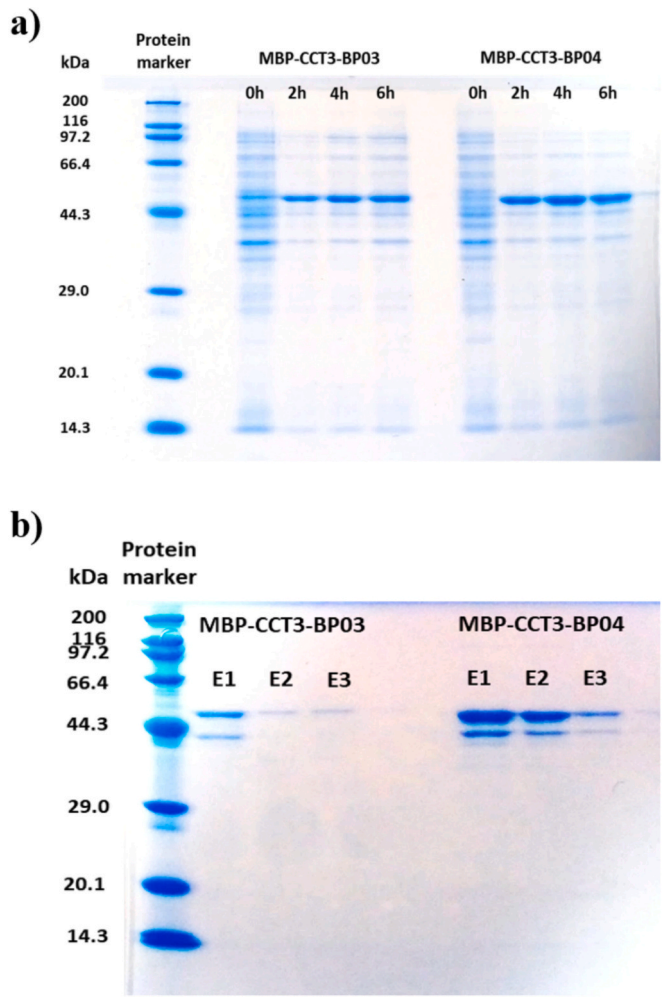

Fig. 3. SDS-PAGE analysis for expression and purification of MBP-fused peptides. a) Expression of MBP-fused binding peptides. Lanes 0 h, 2 h, 4 h, and 6 h in both constructs represent IPTG induction time. b) Purification of MBP–fused binding peptides. Lanes E1–E3 represent the elution fraction number for each construct. The major band for MBP-fused binding peptides is around 48 kDa.

revealed distinct stability profiles between the two constructs. Backbone RMSD analysis showed that MBP–CCT3–BP04 stabilized at a lower deviation relative to its initial structure compared to MBP–CCT3–BP03 (Fig. 2a). RMSF analysis indicated low fluctuations across the MBP domain (residues 1–370) for both systems, suggesting that fusion did not destabilize the overall scaffold (Fig. 2b). Within the peptide region, MBP–CCT3–BP04 exhibited comparatively lower fluctuation amplitudes, indicating more restrained conformational flexibility. The radius of gyration profile of MBP–CCT3–BP04 remained relatively stable throughout the simulation (Fig. 2c), whereas MBP–CCT3–BP03 showed larger fluctuations, suggesting greater conformational expansion. Consistently, solvent-accessible surface area (SASA) values were lower for MBP–CCT3–BP04 (Fig. 2d), indicating a more compact structure. Hydrogen bond analysis further showed that MBP–CCT3–BP04 maintained a higher average number of hydrogen bonds during simulation (Fig. 2e), reflecting good structural cohesion. Collectively, these findings highlight differences in dynamic behavior and structural compactness under solution-phase conditions. The discrepancy between calculated binding energies (favoring MBP–CCT3–BP03) and electrochemical performance (favoring MBP–CCT3–BP04) likely arises from surface-immobilization and orientation effects that are not captured in the current simulation model, underscoring the importance of experimental validation.ptide binding to KIM-1.

3.3. Expression and purification of MBP–CCT3-BP03 and MBP-CCT3-BP04

The recombinant construct was successfully expressed in *E. coli* BL21 (DE3) following the IPTG induction. SDS-PAGE analysis of the soluble fraction showed that both MBP fusion constructs reach maximum expression between 4 and 6 h indicated by a thick band around 48 kDa which correspond to the size of the constructs (Fig. 3a). Consequently, SDS-PAGE analysis of the purification of the soluble fractions yielded the same band around 48 kDa and another visible band around 42 kDa that corresponds with tag-only MBP which was co-purified alongside the fusion constructs (Fig. 3b). Herein, fainter bands of MBP-CCT3-BP03 were noticeable as compared to MBP-CCT3-BP04, which suggested that the former has a lower recovery yield. The purified proteins were subsequently buffer-exchanged into 10 mM PBS (pH 7) for downstream binding affinity assays to avoid potential interference from Tris buffer during surface immobilization [32].

3.4. Experimental determination of apparent affinity constant (K_{app})

The binding of MBP-CCT3-BP03 and MBP-CCT3-BP04 against KIM-1 was evaluated electrochemically using the Langmuir plot which are presented in Fig. S5. The K_{app} calculated between MBP-CCT3-BP03 and MBP-CCT3-BP04 against KIM-1 was 0.079 nM ($R^2 = 0.92$) and 0.13 nM ($R^2 = 0.98$), respectively. The values of K_{app} for both MBP-fused peptides suggested a good binding affinity towards KIM-1, with MBP-CCT3-BP04 displayed stronger binding affinity as compared to MBP-CCT3-BP03. To confirm that the measured interaction was attributed to the designed peptides rather than the fusion tag, MBP alone was evaluated as a control. The calculated K_{app} for MBP was 0.0005 nM ($R^2 = 0.94$), significantly lower than that of the fusion constructs, confirming minimal intrinsic affinity of MBP towards KIM-1. Although computational predictions suggested slightly different relative binding energies between the two constructs, experimental affinity measurements identified MBP–CCT3–BP04 as the stronger binder. Based on these results, MBP–CCT3–BP04 was selected for subsequent biosensor development.

3.5. Electrode fabrication and surface optimization

The KIM-1 biosensor was constructed on the SPCE working electrode (Fig. S6). Following previous reports, the electrode was first modified with MWCNT–chitosan (MWCNT-CS) to enhance conductivity and adhesion [33,34], then coated with 1% starch to enable oriented immobilization of MBP–CCT3–BP04 *via* MBP–polysaccharide affinity. Higher starch concentrations (>2%) caused surface fouling and instability (Fig. S7). Surface saturation of MBP–CCT3–BP04 was quantified by BCA assay, showing maximal immobilization at 15 μM (6.1 ± 0.6 μg); higher concentrations decreased loading due to steric hindrance and partial desorption (Fig. S8a). To reduce non-specific adsorption, electrodes were blocked sequentially with 10 mM PMDA and 1% BSA [35,36]. KIM-1 binding was evaluated across pH 4–7 (Fig. 8b), with maximal response and minimal background at pH 5, consistent with enhanced electrostatic interaction below KIM-1's isoelectric point [37–39].

Stepwise characterization of the modified electrode was achieved through cyclic voltammetry (CV) and electrochemical impedance spectroscopy (EIS) using $K_3Fe(CN)_6/K_4Fe(CN)_6$ redox probe in PBS, scanning between −0.2 and 0.7 V at 0.025 V/s scan rate (Fig. 4a, b). Voltammograms were acquired at each fabrication stage: bare SPCE, MWCNT-CS modification, starch functionalization, MBP-CCT3-BP04 attachment, PMDA and BSA blocking. Modification with MWCNT-CS reduced charge transfer resistance (R_{ct}), from 10,279 Ω to 5000.9 Ω, confirming improved conductivity. Starch deposition slightly increased R_{ct} to 7325 Ω, consistent with formation of a non-conductive film. Immobilization of MBP–CCT3–BP04 further increased resistance due to surface coverage by the protein layer. PMDA treatment decreased R_{ct},

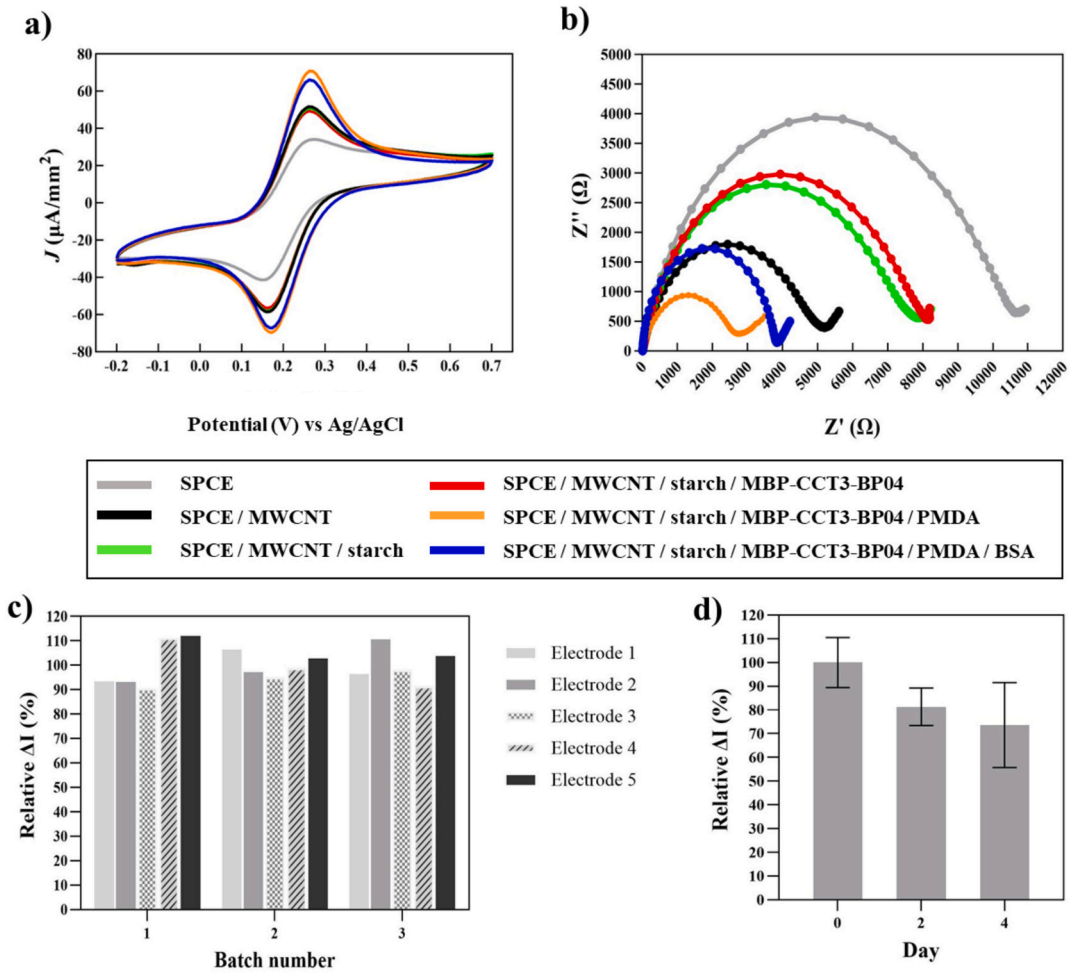

Fig. 4. Electrochemical analysis for optimization of SPCE fabrication. a) Characterization of every layer of the fabricated electrode by CV analysis. b) Nyquist plots of the SPCE during stepwise biosensor fabrication. c) Electrode-to-electrode reproducibility and batch-to-batch variation of the KIM-1 biosensor. Relative responses of five independently fabricated electrodes are shown for two separate fabrication batches ($n = 5$). Error bars represent ± SD, with overall RSD of 10.59% for Batch 1, 4.58% for Batch 2 and 7.29% for Batch 3, indicating excellent reproducibility and fabrication consistency. d) Stability of the KIM-1 biosensor over 4 days of storage at 4 °C. Signal retention is expressed as % relative to Day 0 ($n = 3$). Data are presented as mean ± standard deviation (SD), based on n = 3 replicates.

likely due to improved interfacial charge transfer [40], while final BSA blocking increased resistance, reflecting formation of an insulating protein layer. Based on the obtained voltammogram, the established potential for the fabricated electrode was decided at 0.23 V.

Batch-to-batch evaluation demonstrated that independently fabricated electrodes retained more than 90% of their initial detection response towards KIM-1, indicating good fabrication consistency (Fig. 4c). The relative standard deviation (RSD) values for Day 0, Day 2, and Day 4 were 10.59%, 4.58%, and 7.29%, respectively, confirming acceptable inter-batch precision over the evaluation period. Reproducibility tests using five independently prepared electrodes further showed low signal variation under identical fabrication conditions, with RSD values within 4.58–10.59%, indicating good electrode-to-electrode consistency. The developed biosensor exhibited excellent stability when stored at 4 °C, retaining 81.4% of its activity by day 2 and 73.6% by day 4 (Fig. 4d).

3.6. Detection of KIM-1

The MBP-CCT3-BP04 electrode reliably detected KIM-1 through a decrease in electrochemical current, consistent with the insulating properties of the protein-analyte complex (Fig. 5a) [19]. The lowest tested concentration (1 pg/mL) produced a current density of 4.2 ± 2.0 μA/mm^2, while the maximum concentration (10 ng/mL) caused a 10.9 ± 3.2 μA/mm^2 current density decrease. Linear regression analysis of log-transformed current changes across the concentration range (1 pg/mL to 10 ng/mL) yielded the equation $J = 10.79\ \mathrm{Log_{10}}\ [\mathrm{KIM\text{-}1}] + 39.26$ with excellent correlation ($R^2 = 0.97$) (Fig. 5b). The detection limit was determined to be 1.02 ng/mL using the 3σ/m formula, where σ represents standard deviation and m denotes the calibration gradient. The limit of quantification (LOQ) was calculated to be 3.41 ng/mL using the formula 10σ/m. This sensitivity falls within clinically relevant urinary KIM-1 concentrations associated with early kidney injury [17].

Specificity analysis against CRP, LRG1, EpCAM, and sPLA2 demonstrated reduced responses compared to KIM-1 (Fig. 5c). Although EpCAM exhibited moderate cross-reactivity (50.0% ± 7.8%), the response remained lower than that of KIM-1. Other interferents produced weaker signals (20–40% range). Selectivity was evaluated using relative current change at equivalent molar concentrations (100 pM). In PBS, KIM-1 produced the highest normalized response (100% ± 9.8%, RSD = 9.8%), while non-specific proteins (NSP) generated a lower response (65.9% ± 7.1%, RSD = 10.8%) (Fig. 5d). When KIM-1 was measured in the presence of NSP, the response remained comparable (97.7% ± 9.8%, RSD = 10.0%), indicating preserved recognition under competitive conditions. The blank signal was minimal (5.0% ± 1.01%). These results confirm preferential recognition of KIM-1 by the MBP–CCT3–BP04 receptor. Although molar-normalized selectivity experiments were performed, excess-interferent and competitive mixed-

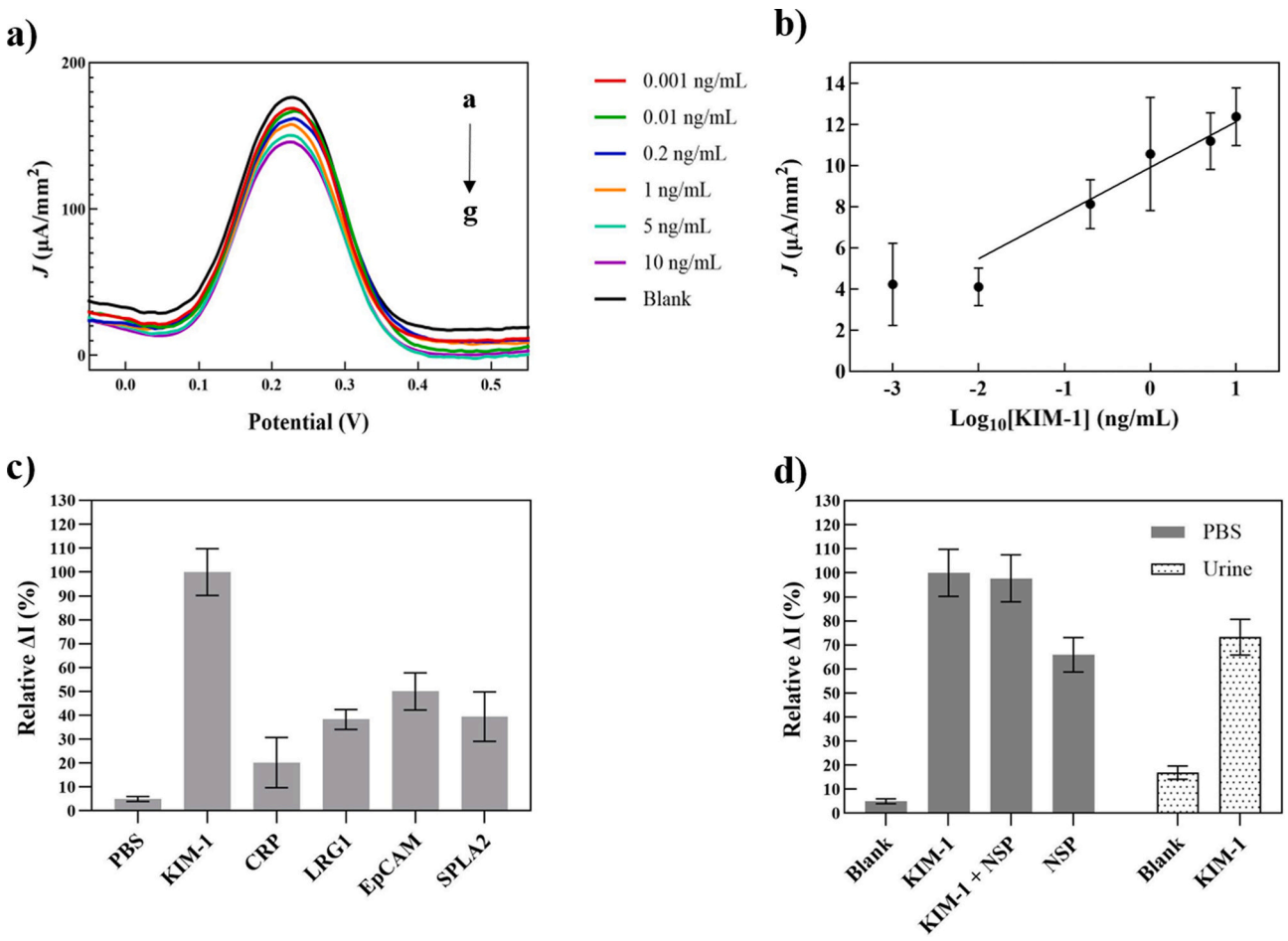

Fig. 5. Electrochemical analysis for the performance of the developed KIM-1 biosensor. a) Square wave voltammetry response of MBP-CCT3-BP04 fabricated biosensor against different concentrations of KIM-1; a – g represents increasing concentration of KIM-1 from blank (PBS) to 10 ng/mL. b) Linear calibration curve of current density (J) against Log_{10} of KIM-1 concentration (ng\mL). c) Specificity analysis for KIM-1 detection against various non-specific proteins (NSP); CRP, LRG1, EpCAM and sPLA2. The concentration of these proteins was standardized to 100 pM. d) Selectivity of MBP-CCT3-BP04 against KIM-1 in buffer spiked with various NSPs and in simulated urine sample. Data are presented as relative ΔI ± standard deviation (SD), based on $n = 3$ replicates.

Table 3
Previously developed KIM-1 biosensor in literatures.

Sensor classification	Bioreceptor	Linear range	LOD	Sample	Notable feature	References
Electrochemical biosensor	MBP-fused CCT3-based peptides	1–10,000 pg/mL	1.02 ng/mL	Urine	Peptide receptor, affinity peptide design, high stability, low cost	This work
Molecular imaging	Phage-displayed 6-amino acids peptides (CNRRRA)	n/s	n/s	*In vivo*	Synthetic peptide, high stability, KIM-1 concentration-independent	[41]
Molecular imaging and multimodal read-outs	SPION nanoprobes conjugated LTH peptides (LTHVVWL)	n/s	n/s	*In vivo* (renal tubular cells)	Synthetic peptide, high stability, KIM-1 concentration-independent	[42]
Electrochemical immunosensor	Anti-KIM-1 antibody	0.1–1000 ng/ml	64 pg/ml	Serum	Costly gold-nano dendrites, laborious fabrication processes	[43]
Electrochemical immunosensor	Anti-KIM-1 antibody	0.01–50.00 pg/mL	2.00 fg/mL	Blood plasma	Highly sensitive, use 2 types of antibody	[44]
Electrochemical biosensor	Anti-KIM-1 antibody	0.1–1000 fg/ mL	0.26 fg/mL	Urine	Ultra-sensitive immunosensor in urine, ITO-PET electrode is costly	[45]
Electrochemical biosensor	Anti-KIM-1 antibody	100 pg/mL to 100 ng/mL	32 pg/mL	Urine	Sensitive protein assays, Long incubation time (60 mins)	[46]

n/s = not specified. The author does not report the LOD and linear range of their work.
Abbreviation: SPION (superparamagnetic iron oxide nanoparticles).

sample conditions were not investigated in this study. Future work will evaluate sensor robustness under elevated interferent concentrations to further validate clinical applicability.

3.7. Evaluation of the performance of the developed biosensor

The electrode's performance was further validated using artificial urine prepared according to Sarigul et al.'s protocol [29], spiked with 1 ng/mL KIM-1 to simulate pathological conditions. Following the optimized conditions, the developed biosensor has successfully detected

KIM-1 in simulated urine sample, generating a substantial signal response (73.3% ± 7.4%, RSD = 10.1%), significantly higher than the urine blank (16.9% ± 2.7%), confirming matrix compatibility (Fig. 5c). A comparison with previously reported KIM-1 biosensors is summarized in Table 3. Most reported systems employ antibody-based recognition elements, achieving very low detection limits but often involving higher production cost and potential stability limitations. In contrast, the present work demonstrates a computationally guided peptide receptor integrated into a straightforward electrochemical platform. While the achieved LOD does not reach the lowest values reported for antibody-based systems, the proposed approach offers advantages in receptor design flexibility, structural robustness, and surface immobilization strategy. These features highlight the potential of peptide-based bioreceptors as viable alternatives for practical and scalable KIM-1 biosensing applications.

4. Conclusion and future recommendations

This study presents a proof-of-concept demonstration that computationally designed peptides derived from CCT3 can serve as functional recognition elements for KIM-1 detection. To the best of our knowledge, beyond the mass spectrometry investigation by Yang et al., this is the first work exploring the interaction between CCT3-derived sequences and KIM-1 for biosensing applications. A peptide candidate (CCT3-BP04) was rationally designed through molecular docking and molecular dynamics simulations, fused with MBP for controlled immobilization, and successfully integrated into an electrochemical sensing platform. Under optimized conditions, the biosensor exhibited concentration-dependent signal responses corresponding to the apparent surface binding affinity of MBP–CCT3–BP04 towards KIM-1. It should be noted that the reported affinity values represent surface-confined interactions influenced by MBP fusion and electrode interface effects, rather than intrinsic thermodynamic constants measured in solution. The starch intermediate layer was employed to exploit the natural affinity between MBP and polysaccharides, enabling mild and potentially oriented immobilization; however, starch-free immobilization strategies were not investigated in this study and remain an area for future exploration.

The system further demonstrated selective detection in both buffered solutions and simulated urine samples, confirming functional performance in complex matrices. Although the achieved detection limit does not surpass the lowest values reported for antibody-based systems, the present work highlights an alternative receptor strategy that emphasizes design flexibility, structural robustness, and simplified fabrication. These findings establish a foundational framework for integrating computational peptide design with electrochemical biosensor development. Future refinement through sequence optimization, structure-guided mutagenesis, and extended simulation strategies may further enhance binding affinity and analytical performance. Overall, this study demonstrates that computationally guided peptide engineering represents a viable and efficient approach for advancing next-generation biosensor receptor development.

CRediT authorship contribution statement

Muhammad Syafiq Mohd Razib: Writing – review & editing, Writing – original draft, Visualization, Validation, Methodology, Investigation, Formal analysis, Data curation, Conceptualization. **Shoko Tanaka:** Writing – review & editing, Validation, Investigation, Formal analysis, Data curation. **Noor Syamila:** Writing – review & editing, Validation, Formal analysis, Data curation. **Muhamad Arif Mohamad Jamali:** Writing – review & editing, Resources, Methodology. **Amir Syahir Amir Hamzah:** Writing – review & editing, Resources, Conceptualization. **Shinya Ikeno:** Writing – review & editing, Validation, Supervision, Resources, Project administration, Methodology, Investigation, Funding acquisition, Formal analysis, Conceptualization.

Declaration of competing interest

The authors declare the following financial interests/personal relationships which may be considered as potential competing interests: The authors declare the following financial interests/personal relationships which may be considered as potential competing interests: Noor Syamila reports financial support was provided by Biogenes Technologies Sdn Bhd. Noor Syamila reports a relationship with Biogenes Technologies Sdn Bhd that includes: employment. Shinya Ikeno reports a relationship with Biogenes Technologies Sdn Bhd that includes: funding grants. If there are other authors, they declare that they have no known competing financial interests or personal relationships that could have appeared to influence the work reported in this paper.

Acknowledgments

The authors sincerely acknowledge the invaluable support and collaboration between Kyushu Institute of Technology (KYUTECH) and Universiti Putra Malaysia (UPM), whose joint efforts greatly facilitated the successful completion of this research.

Appendix A. Supplementary data

Supplementary data to this article can be found online at https://doi.org/10.1016/j.microc.2026.118092.

Data availability

Data will be made available on request.

References

[1] M. Snelson, et al., Long term high protein diet feeding alters the microbiome and increases intestinal permeability, systemic inflammation and kidney injury in mice, Mol. Nutr. Food Res. 65 (8) (2021), https://doi.org/10.1002/mnfr.202000851.
[2] A. Francis, et al., Chronic kidney disease and the global public health agenda: an international consensus, Nat. Rev. Nephrol. 20 (7) (2024) 473–485, https://doi.org/10.1038/s41581-024-00820-6.
[3] M. Kumar, et al., The bidirectional link between diabetes and kidney disease: mechanisms and management, Cureus (2023), https://doi.org/10.7759/cureus.45615.
[4] H. Tan, et al., Global burden and trends of high BMI-attributable chronic kidney disease: a comprehensive analysis from 1990 to 2021 and projections to 2035, Front. Nutr. 12 (2025), https://doi.org/10.3389/fnut.2025.1611227.
[5] M.J. Li, H.Y. Liu, Y.Q. Zhang, S.R. Li, J.H. Zhang, R. Li, Global burden of chronic kidney disease and its attributable risk factors (1990-2021): an analysis based on the global burden of disease study, Front. Endocrinol. (Lausanne) 16 (2025), https://doi.org/10.3389/fendo.2025.1563246.
[6] C.P. Kovesdy, Epidemiology of chronic kidney disease: an update 2022, Kidney International Supplements (2022), https://doi.org/10.1016/j.kisu.2021.11.003.
[7] V. Jha, et al., Global economic burden associated with chronic kidney disease: a pragmatic review of medical costs for the inside CKD research programme, Adv. Ther. 40 (10) (2023) 4405–4420, https://doi.org/10.1007/s12325-023-02608-9.
[8] R. Borg, N. Carlson, J. Søndergaard, F. Persson, The growing challenge of chronic kidney disease: an overview of current knowledge, International Journal of Nephrology (2023), https://doi.org/10.1155/2023/9609266.
[9] D.J. Oh, A long journey for acute kidney injury biomarkers, Renal Failure (2020), https://doi.org/10.1080/0886022X.2020.1721300.
[10] E.M. Templeton, et al., Identifying candidate protein markers of acute kidney injury in acute decompensated heart failure, Int. J. Mol. Sci. 23 (2) (2022), https://doi.org/10.3390/ijms23021009.
[11] C.W. Lin, et al., Application of a novel biosensor for salivary conductivity in detecting chronic kidney disease, Biosensors (Basel). 12 (3) (2022), https://doi.org/10.3390/bios12030178.
[12] M. Mizdrak, M. Kumrić, T.T. Kurir, J. Božić, Emerging biomarkers for early detection of chronic kidney disease, Journal of Personalized Medicine (2022), https://doi.org/10.3390/jpm12040548.
[13] C.-F. Zhang, et al., The diagnostic and prognostic values of serum and urinary kidney injury molecule-1 and neutrophil gelatinase-associated lipocalin in sepsis induced acute renal injury patients, Eur. Rev. Med. Pharmacol. Sci. 24 (10) (2020) 5604–5617, https://doi.org/10.26355/eurrev_202005_21346.
[14] C. Yang, et al., Kidney injury molecule-1 is a potential receptor for SARS-CoV-2, J. Mol. Cell Biol. 13 (3) (2021) 185–196, https://doi.org/10.1093/jmcb/mjab003.
[15] B. Brilland, et al., Kidney injury molecule 1 (KIM-1): a potential biomarker of acute kidney injury and tubulointerstitial injury in patients with ANCA-

glomerulonephritis, Clin. Kidney J. 16 (9) (2023) 1521–1533, https://doi.org/10.1093/ckj/sfad071.
[16] J. Geng, Y. Qiu, Z. Qin, B. Su, The value of kidney injury molecule 1 in predicting acute kidney injury in adult patients: a systematic review and Bayesian meta-analysis, Journal of Translational Medicine (1) (2021), https://doi.org/10.1186/s12967-021-02776-8.
[17] K. Seitkamal, et al., Sensitive detection of kidney injury biomarker (KIM1) in urine samples using an optical fiber semi-distributed interferometer biosensor, Talanta 295 (2025), https://doi.org/10.1016/j.talanta.2025.128348.
[18] V. Naresh, N. Lee, A review on biosensors and recent development of nanostructured materials-enabled biosensors, Sensors (2021), https://doi.org/10.3390/s21041109.
[19] E.C. Ankara, S. Aras, B. Demirbakan, M.K. Sezgintürk, Fabrication of ultra-sensitive and disposable electrochemical biosensor: detection of kidney injury molecule-1 protein in urine for diagnosis of kidney injury, Journal of Pharmaceutical and Biomedical Analysis Open 4 (2024), https://doi.org/10.1016/j.jpbao.2024.100042.
[20] B. Natarajan, P. Kannan, P. Subramanian, G. Maduraiveeran, Metal nanoparticles based electrochemical biosensing of neutrophil gelatinase-associated lipocalin biomarker for monitoring acute kidney injury, Microchemical Journal (2024), https://doi.org/10.1016/j.microc.2024.110890.
[21] J.H. Kim, et al., Harnessing protein sensing ability of electrochemical biosensors via a controlled peptide receptor–electrode interface, J. Nanobiotechnology 21 (1) (2023), https://doi.org/10.1186/s12951-023-01843-0.
[22] C. Yang, et al., A renal YY1-KIM1-DR5 axis regulates the progression of acute kidney injury, Nat. Commun. 14 (1) (2023), https://doi.org/10.1038/s41467-023-40036-z.
[23] A. Alhossary, S.D. Handoko, Y. Mu, C.K. Kwoh, Fast, accurate, and reliable molecular docking with QuickVina 2, Bioinformatics 31 (13) (2015) 2214–2216, https://doi.org/10.1093/bioinformatics/btv082.
[24] B.R. Brooks, et al., CHARMM: the biomolecular simulation program, J. Comput. Chem. 30 (10) (2009) 1545–1614, https://doi.org/10.1002/jcc.21287.
[25] J. Lee, et al., CHARMM-GUI input generator for NAMD, GROMACS, AMBER, OpenMM, and CHARMM/OpenMM simulations using the CHARMM36 additive force field, J. Chem. Theory Comput. 12 (1) (2016) 405–413, https://doi.org/10.1021/acs.jctc.5b00935.
[26] S. Jo, T. Kim, V.G. Iyer, W. Im, CHARMM-GUI: a web-based graphical user interface for CHARMM, J. Comput. Chem. 29 (11) (2008) 1859–1865, https://doi.org/10.1002/jcc.20945.
[27] G. Aylaz, M. Andaç, Affinity-recognition-based gravimetric nanosensor for equilin detection, Chemosensors 10 (5) (2022), https://doi.org/10.3390/chemosensors10050172.
[28] B. McCann, B. Tipper, S. Shahbeigi, M. Soleimani, M. Jabbari, M. Nasr Esfahani, A Review on Perception of Binding Kinetics in Affinity Biosensors: Challenges and Opportunities, Am. Chem. Soc. (2025), https://doi.org/10.1021/acsomega.4c10040.
[29] N. Sarigul, F. Korkmaz, İ. Kurultak, A new artificial urine protocol to better imitate human urine, Sci. Rep. 9 (1) (2019), https://doi.org/10.1038/s41598-019-56693-4.
[30] H. Kim, J. Park, S.H. Roh, The structural basis of eukaryotic chaperonin TRiC/CCT: action and folding, Molecules and Cells (2024), https://doi.org/10.1016/j.mocell.2024.100012.
[31] M. Srisaisap, T. Suwankhajit, P. Boonserm, A fusion protein designed for soluble expression, rapid purification, and enhanced stability of parasporin-2 with potential therapeutic applications, Biotechnology Reports 43 (2024), https://doi.org/10.1016/j.btre.2024.e00851.
[32] Y.H. Cheng, C. Chande, Z. Li, N. Haridas Menon, S. Kaaliveetil, S. Basuray, Optimization of electrolytes with redox reagents to improve the impedimetric signal for use with a low-cost analyzer, Biosensors (Basel). 13 (12) (2023), https://doi.org/10.3390/bios13120999.
[33] F.A. Azri, R. Sukor, J. Selamat, F.A. Bakar, N.A. Yusof, R. Hajian, Electrochemical immunosensor for detection of aflatoxin b 1 based on indirect competitive ELISA, Toxins (Basel). 10 (5) (2018), https://doi.org/10.3390/toxins10050196.
[34] F.A. Azri, R. Sukor, R. Hajian, N.A. Yusof, F.A. Bakar, J. Selamat, Modification strategy of screen-printed carbon electrode with functionalized multi-walled carbon nanotube and chitosan matrix for biosensor development, Asian J. Chem. 29 (1) (2017) 31–36, https://doi.org/10.14233/ajchem.2017.20104.
[35] B. Bachour Junior, M.R. Batistuti, A.S. Pereira, E.M. de Sousa Russo, M. Mulato, Electrochemical aptasensor for NS1 detection: towards a fast dengue biosensor, Talanta 233 (2021), https://doi.org/10.1016/j.talanta.2021.122527.
[36] S.H. Shamsuddin, T.D. Gibson, D.C. Tomlinson, M.J. McPherson, D.G. Jayne, P. A. Millner, Reagentless affimer- and antibody-based impedimetric biosensors for CEA-detection using a novel non-conducting polymer, Biosens. Bioelectron. 178 (2021), https://doi.org/10.1016/j.bios.2021.113013.
[37] K. Talley, C. Ng, M. Shoppell, P. Kundrotas, E. Alexov, On the electrostatic component of protein-protein binding free energy, PMC Biophys. 1 (1) (2008), https://doi.org/10.1186/1757-5036-1-2.
[38] S.T. Moerz, P. Huber, PH-dependent selective protein adsorption into mesoporous silica, J. Phys. Chem. C 119 (48) (2015) 27072–27079, https://doi.org/10.1021/acs.jpcc.5b09606.
[39] Q. Tan, Y. Kan, H. Huang, W. Wu, X. Lu, Probing the molecular interactions of chitosan films in acidic solutions with different salt ions, Coatings 10 (11) (2020) 1–14, https://doi.org/10.3390/coatings10111052.
[40] K. Takizawa, S. Asai, S. Ando, Temperature dependence of electric conduction in polyimides with main chain triphenylamine structures, Polym. J. 46 (4) (2014) 201–206, https://doi.org/10.1038/pj.2013.93.
[41] T.J. Kwon, et al., Development of a noninvasive KIM-1-based live-imaging technique in the context of a drug-induced kidney-injury mouse model, ACS Appl. Bio Mater. 4 (2) (2021) 1508–1514, https://doi.org/10.1021/acsabm.0c01392.
[42] Q. Chen, J. Yang, M. Yang, Z. Luo, Y. Lei, Q. Zhang, Kim-1-targeted multimodal nanoprobes for early diagnosis and monitoring of sepsis-induced acute kidney injury, Apoptosis (2025), https://doi.org/10.1007/s10495-025-02141-w.
[43] M. Das, T. Chakraborty, C. Yu Lin, K. Fong Lei, C. Haur Kao, Hierarchical gold-Galinstan nanodendrites modified disposable immunosensor for the label-free detection of KIM-1 by antibody immobilization on staphylococcal protein a, Appl. Surf. Sci. 607 (2023), https://doi.org/10.1016/j.apsusc.2022.154930.
[44] H. Boyacıoğlu, B.B. Yola, C. Karaman, O. Karaman, N. Atar, M.L. Yola, A novel electrochemical kidney injury molecule-1 (KIM-1) immunosensor based covalent organic frameworks-gold nanoparticles composite and porous NiCo2S4@CeO2 microspheres: the monitoring of acute kidney injury, Appl. Surf. Sci. 578 (2022), https://doi.org/10.1016/j.apsusc.2021.152093.
[45] E.C. Ankara, S. Aras, B. Demirbakan, M.K. Sezgintürk, Fabrication of ultra-sensitive and disposable electrochemical biosensor: detection of kidney injury molecule-1 protein in urine for diagnosis of kidney injury, Journal of Pharmaceutical and Biomedical Analysis Open 4 (2024), https://doi.org/10.1016/j.jpbao.2024.100042.
[46] Z. Yin, C. Liu, Y. Yi, H. Wu, X. Fu, Y. Yan, A label-free electrochemical immunosensor based on PdPtCu@BP bilayer nanosheets for point-of-care kidney injury molecule-1 testing, J. Electroanal. Chem. 917 (2022), https://doi.org/10.1016/j.jelechem.2022.116420.